Int. J. Therm. Sci. (2001) 40, 104–113

S1290-0729(00)01199-6/FLA

Radiation emitted from fluidizing particles adjacent to a heated surface in a fluidized bed

Jun Yamada [a]*, Yasuo Kurosaki [b], Tomoyuki Morikawa [c]

[a] *Department of Mechanical System Engineering, Yamanashi University, Takeda 4, Kofu, Yamanashi 400-8511, Japan*

[b] *Department of Mechanical and Control Engineering, University of Electro-Communications, Chofugaoka 1, Chofu, Tokyo 182-8585, Japan*

[c] *Energy Technology Department, Kubota Corporation, Hama 1-1-1, Amagasaki, Hyogo 661, Japan*

(Received 29 November 1999, accepted 29 February 2000)

Abstract — We experimentally investigated the radiation heat exchange occurring in a gas–solid fluidized bed (kept at 25 °C) between the fluidizing particles and a remotely-heated heat transfer surface (30 °C). To evaluate this heat exchange, radiation emitted from the fluidizing particles towards the heated surface was measured through a transparent heat transfer surface using an infrared imager. Our experimental results revealed that the fluidizing particles are mainly heated by conduction during the contact period with the surface and/or by gas convection in the thermal boundary layer, and that these heated particles frequently emit a significant amount of radiation energy toward the surface. Based on these results, a method for evaluating the radiation heat exchange between the heat transfer surface and the fluidizing particles is proposed. The proposed method shows that particle diameter is one of the most significant parameters in the radiation heat exchange, and predicts that the radiation heat exchange increases with increasing particle diameter. © 2001 Éditions scientifiques et médicales Elsevier SAS

fluidized bed / radiative heat transfer / visualization / heat exchanger / dispersed medium / radiation / heat transfer

Nomenclature

d	particle diameter	m
E	radiative energy flux emitted from the fluidizing bed	$W \cdot m^{-2}$
E_b	radiative energy flux emitted from the blackbody	$W \cdot m^{-2}$
E_s	radiative energy flux emitted from the infrared imager sensor	$W \cdot m^{-2}$
T_{sur}	surroundings temperature (20 °C)	
T_{in}	inlet gas temperature (20 °C)	
T_w	temperature of the heat transfer surface (30 °C)	
T_{bed}	bed temperature outside the thermal boundary layer on the heat transfer surface (25 °C or 30 °C)	
U	fluidizing velocity	$m \cdot s^{-1}$
U_{mf}	minimum fluidizing velocity	$m \cdot s^{-1}$
D	system output of the measured radiation energy emitted from the fluidizing bed	
D_b	system output of the measured radiation energy emitted from the blackbody	
$D_{iso\text{-}bed}$	system output of the measured radiation energy emitted from an isothermal bed	
ε_{bed}	bed emissivity	
Ψ	efficiency of the radiation heat exchange	

* Correspondence and reprints.
E-mail address: jyamada@ccn.yamanashi.ac.jp (J. Yamada).

1. INTRODUCTION

Fluidized beds are conventionally used in high-temperature heat exchanger applications such as chemical reactors and coal combustors due to their excellent heat transfer performance. In these type of applications, the radiation transfer between the fluidized particles and the heat transfer surface is considered to be a significant heat transfer mechanism. However, even though much effort has been directed at clarifying the radiation transfer mechanism in fluidized beds [1–6], questions remain concerning the effects of (1) the fluidizing velocities, (2) the optical characteristics of the particles, and (3) the particle diameter on the radiation transfer [7].

We previously carried out optical experiments employing a He–Ne laser and a corresponding numerical simulation analysis [8]. We then proposed a model for predicting the radiation heat exchange occurring between fluidized particles and a heat transfer surface which takes into account the thermal boundary layer on the heat transfer surface.

When the radiation heat exchange was occurring between fluidizing particles and a heat transfer surface whose temperature is higher than the bed temperature, our model predicts that radiation heat transfer is not enhanced when the penetration depth of radiation is less than the thickness of the thermal boundary layer. This may occur because the fluidizing particles adjacent to the heat transfer surface are heated by conduction while in contact with the surface and/or by gas convection in the thermal boundary layer, and consequently, they emit radiation which cancels that which is emitted from the heated surface (*figure 1*). On the other hand, when the penetration depth is greater than the thermal boundary layer, the layer's optical thickness where the heated particles exist is thin, and the amount of radiation energy emitted by the heated particles is always small. In this case, the radiation heat exchange between the fluidizing particles and the surface is efficient. Associated heat transfer experiments supported this prediction in part [8].

It should be noted that the former phenomenon was derived assuming that the temperature of particles adjacent to the heat transfer surface were equal to the gas temperature. However, since the particles are transiently heated by direct-contact heat exchange between the surface and the particles during the contact period and/or by convective heat transfer from flowing gas in the thermal boundary layer, it is not reasonable to assume that the temperature of the particles was equal to the gas temperature. Furthermore, it is not empirically known whether such heated particles actually exist near the heated surface, or how much radiation they emit.

This leads to the present study which specifically investigates the radiation emitted from the fluidizing particles in order to evaluate the radiation heat exchange taking place between these particles and the heat transfer surface. We present a visualization technique for the temperature of particles using an infrared (IR) imager to confirm the presence of the heated particles. We used it to measure the time-averaged radiation energy being emitted from the heated particles in order to evaluate the radiation heat exchange.

The visualization and measurement were performed through a transparent window that also functioned as a heat transfer surface. These measurements reveal that

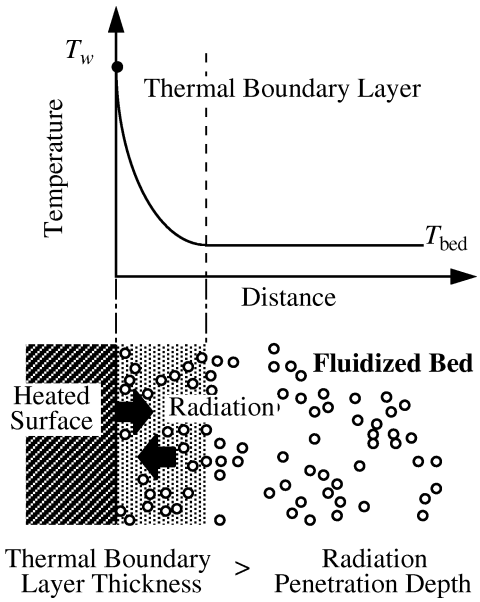

Figure 1. Radiation heat exchange occurring between fluidizing particles and a heated surface.

the heated particles actually exist near the heat transfer surface and frequently emit a significant amount of radiation energy toward the surface, which suppresses the radiation heat exchange between the surface and the fluidizing particles. Furthermore, based on these results, a method for evaluating the radiation heat exchange is discussed.

2. EXPERIMENTAL SETUP AND PROCEDURE

2.1. Experimental fluidized bed

A schematic diagram of the experimental setup is shown in *figure 2*. The experimental fluidized bed has a cross section of 100×100 mm^2 and a height of 1 000 mm. A heat transfer surface having a diameter of 50 mm is located 60 mm above the felt sheet distributor placed at the bottom of the bed. A cartridge heater was immersed in the bed to control the bed temperature.

An IR imager (TVS-2000, Nippon Avionics) located external to the bed was used to visualize the temperature of the fluidizing particles heated by the heat transfer surface, as well as to measure the radiation energy emitted by the particles without disturbing the bed fluidization. A CO_2 laser (NAL-10D, Nippon Kagaku Engineering Co.) was used to remotely heat the heat transfer

surface without obstructing the IR imager. The CO_2 laser was situated normal to the heat transfer surface and the IR imager was slightly tilted away from the axis, as shown in *figure 2*.

A transparent MgF_2 window, which has a diameter of 50 mm and a thickness of 5 mm, acted as the heat transfer surface. Its transparency is more than 95 % in the imager's range of detectable wavelength (3.0–5.4 μm), while it is opaque at the laser's wavelength (10.6 μm).

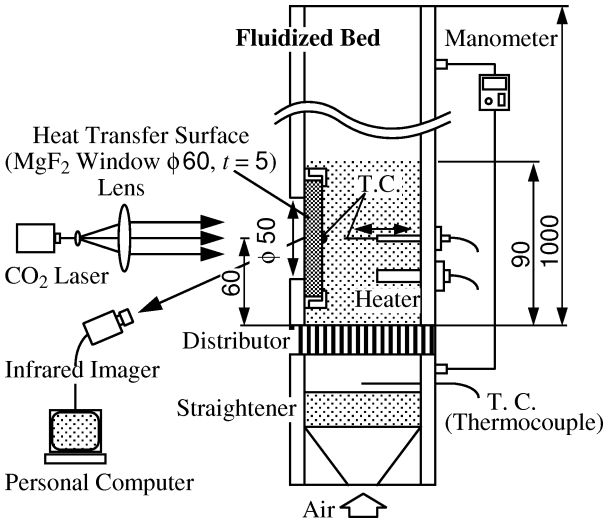

Figure 2. Schematic diagram of the experimental setup.

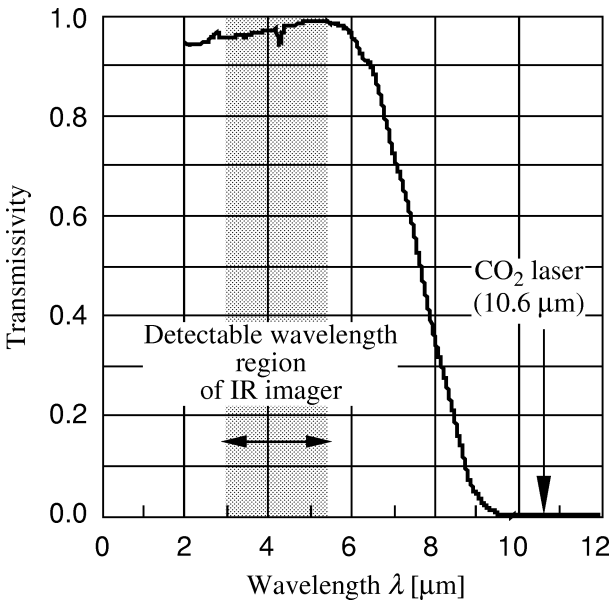

Figure 3. Spectral transmissivity for the normal incidence of MgF_2 window.

The spectral transmissivity for the normal incidence of the MgF_2 window is shown in *figure 3*.

We experimentally confirmed that the window emits negligible radiation in the detectable wavelength region, even during laser heating. Thus, this visualization system allows measurement of only the radiation emitted from the fluidizing particles adjacent to the heat transfer surface.

The IR imager contains an InSb sensor. After translating the measured distribution of radiation energy, a 256 × 100 pixel thermal image with an 8-bit gray scale was produced and this thermal image was stored as digital data. To obtain the original distribution of radiation energy, a personal computer was used to retranslate the thermal image pixel by pixel back to the radiation energy. Since the translation and re-translation between the radiation energy and the temperature are numerically performed, no error is produced.

2.2. Experimental condition and fluidizing particles

The heat transfer surface temperatures T_w was measured by a chromel–alumel (CA) thermocouple having a diameter of 0.1 mm, which is located at the center of the surface. The bed temperature T_{bed}, which is the temperature outside the thermal boundary layer on the surface, was measured by another CA thermocouple located at the height of the heat transfer surface, as shown in *figure 1*. Except the bed emissivity measurement which is described below, all experiments were carried out at a surface temperature T_w of 30 °C and at a bed temperature T_{bed} of 25 °C. The surface temperature and the bed temperature were respectively controlled by the CO_2 laser and by the cartridge heater immersed in the bed.

The static bed height was fixed at 90 mm and the fluidizing velocity U was varied between 1.2 and $3.0U_{mf}$, where U_{mf} is the minimum fluidizing velocity empirically determined by measuring the pressure drop across the bed.

Table I presents the parameters associated with the fluidizing particles used in this study, as well as their corresponding values of U_{mf} and bed emissivity ε_{bed}.

2.3. Measurement of bed emissivity

ε_{bed} is defined as the ratio of the radiation energy emitted from the isothermal, optically thick bed to the black-

TABLE I
Parameters associated with the employed fluidizing particles.

Particle	Diameter [μm]	U_{mf} [m·s^{-1}]	ε_{bed}
Glass	50	0.013	0.79 ± 0.02
	200	0.048	0.89 ± 0.02
	400	0.128	0.90 ± 0.02
Zircon sand	150	0.043	0.72 ± 0.02
Al_2O_3	500	0.284	0.47 ± 0.03

body radiation energy emitted at the bed temperature.[1] This parameter was also empirically determined, i.e. the IR imager was used to measure the radiation energy from the bed and that from a reference blackbody.

In the emissivity measurement, to ensure that the fluidizing particles were not cooled by the heat transfer surface, the bed was isothermally heated by the cartridge heater to 30 °C, while the CO_2 laser was used to maintain the heat transfer surface at the same temperature.

Since the measured radiation contains the radiation from the bed and also from the reflected background radiation at surroundings temperature, T_{sur}, which was 20 °C throughout the entire experiment, it was necessary to correct for the reflected background radiation.

The method used to make the correction is as follows. The signal output of the measurement system is proportional to the amount of measured radiation energy. Using the proportionality constant C, the outputs for radiation energy from the isothermal bed and blackbody can be respectively expressed as

$$D_{\text{iso-bed}} = C\left[\varepsilon_{bed} E_b(T_{bed}) + (1-\varepsilon_{bed}) E_b(T_{sur}) - E_s\right] \tag{1}$$

$$D_b(T_{ref}) = C\left[E_b(T_{ref}) - E_s\right] \tag{2}$$

where $E_b(T)$ is the amount of sensor-detected radiative energy flux emitted from the blackbody at temperature T. The first term on the right-hand side of equation (1) represents the radiation emitted from the isothermal bed at T_{bed}, while the second term represents the reflected background radiation at T_{sur}. The radiative energy flux emitted from the sensor, E_s, was not considered here because the sensor temperature was very low (< 233 K). The first term on the right-hand side of equation (2) represents the radiation emitted from the reference blackbody at T_{ref}.

Using equations (1) and (2), the following equation was derived and utilized to determine the value of ε_{bed} listed in *table I*:

$$\varepsilon_{bed} = \frac{D_{\text{iso-bed}}/D_b(T_{ref}) - E_b(T_{sur})/E_b(T_{ref})}{E_b(T_{bed})/E_b(T_{ref}) - E_b(T_{sur})/E_b(T_{ref})} \tag{3}$$

Here, only $D_{\text{iso-bed}}$ and $D_b(T_{ref})$ were measured to estimate ε_{bed}. The values of $E_b(T)$ were given by the calibration table of the IR imager, which are used for translating the measured radiation energy to a temperature. For $E_b(T)$ that are determined by use of the calibration table, the temperature is specified, for example, $E_b(T_{ref} = 30\,°C)$. According to this expression, equation (3) can be rewritten by

$$\varepsilon_{bed} = \left[\frac{D_{\text{iso-bed}}}{D_b(T_{ref})} - \frac{E_b(T_{sur} = 20\,°C)}{E_b(T_{ref} = 30\,°C)}\right] \cdot \left[1 - \frac{E_b(T_{sur} = 20\,°C)}{E_b(T_{ref} = 30\,°C)}\right]^{-1} \tag{4}$$

where, since T_{bed} is equal to T_{ref} in the bed emissivity measurement, $E_b(T_{bed})/E_b(T_{ref})$ in the denominator of equation (3) is unity.

In the other measurements as well as the bed emissivity measurement, T_w, T_{bed}, T_{ref} and T_{sur} fluctuate around the set temperatures. This fluctuation affects the measured values of $D_{\text{iso-bed}}$, $D_b(T_{ref})$ and D, which will appear in equation (5). The effect of the temperature fluctuations on the estimated value of ε_{bed} and the other radiation parameters is described in appendix.

In this study, because all radiation measurements were carried out using the imager, not only ε_{bed} but the other radiation parameters were also evaluated in the imager's range of detectable wavelengths. It is considered that the significant wavelength range in the radiation heat transfer of practical fluidizing beds, which is usually operated at high temperature, does not match the present range. It should be realized, however, that the results obtained here are applicable to any other fluidizing bed if the radiative parameters are replaced by those in the wavelength range of interest. The applicability to a high-temperature fluidized bed will be discussed later.

[1] ε_{bed} defined in this study is independent of the volume fraction of the bed, which varies with fluidizing velocity. This reason is as follows. The albedo and scattering phase function of a dispersed medium is constant, being independent of its void fraction under the assumption of independent scattering [9], and only the extinction coefficient is proportional to the void fraction. However, since the emissivity of an isothermal optically thick, dispersed medium does not depend on the extinction coefficient [10], the emissivity of such medium is independent of its void fraction and is constant.

3. RESULTS AND DISCUSSION

Experiments were performed at various fluidizing velocities, with bubbling fluidization being observed under all experimental conditions.

3.1. Visualization results of the particles' temperature

Figure 4 shows typical time-dependent photographs of the thermal images of the fluidizing particles located near the heat transfer surface, where the outer circle indicates the transparent heat transfer surface. The temperature indicated in *figure 4* is not the actual temperature of the fluidizing particles because these thermal images are obtained by fixing the bed emissivity at unity. However, these thermal images indicate the temperature in the bright region is higher than that in the dark region.

The dark region in *figure 4(a)* indicates a bubble rising along the surface. Bubbles appear dark because low-temperature fluidizing particles can be seen through them. After the bubble has gone, the low-temperature fluidizing particles come in contact with the heat transfer surface (*figure 4(b)*) and are transiently heated by conduction during the contact period with the surface and/or by gas convection in the thermal boundary layer (*figure 4(c)*). These results prove that heated fluidizing particles exist adjacent to the heat transfer surface.

3.2. Radiation energy emitted by fluidizing particles

The radiation emitted from the fluidizing particles varies because they are transiently heated and leave the heat transfer area. Thus, for practical purposes, the time-averaged radiation energy emitted from the heated particles is required to evaluate the radiation heat transfer occurring between the fluidizing particles and heat transfer surface. We derived the time-averaged radiation energy using 40 thermal images taken at 10 s intervals. In the averaging process, all thermal images were translated into radiation energy images, which were then averaged pixel by pixel and retranslated back into a thermal image. A photograph of the resultant thermal image is shown in *figure 5*, where the temperature is indicated by fixing the bed emissivity at unity.

Note that the radiation energy from the lower part of the heat transfer surface is less than that of the upper

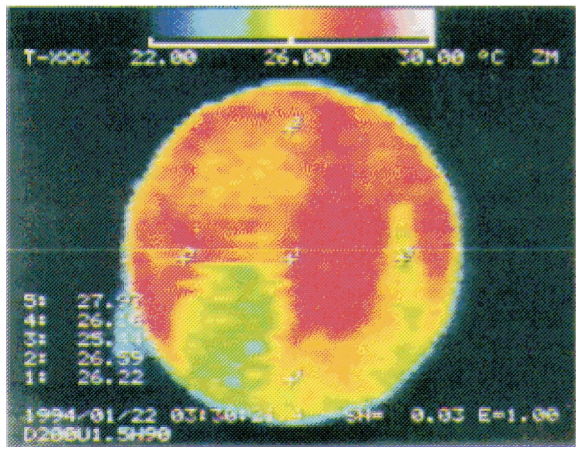

(a)

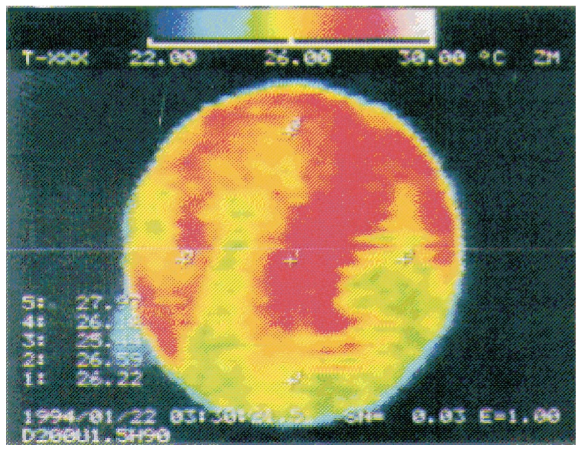

(b)

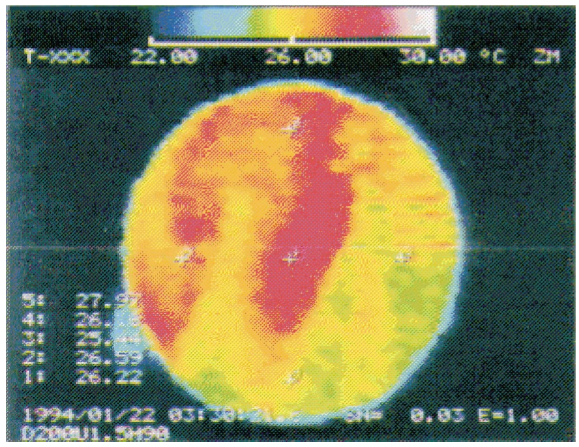

(c)

Figure 4. Thermal images of the heated fluidizing particles located near the heat transfer surface (glass particles, $d = 200$ μm, $U = 1.5U_{mf}$). (a) $t = 0$ s, (b) $t = 0.1$ s, (c) $t = 0.2$ s.

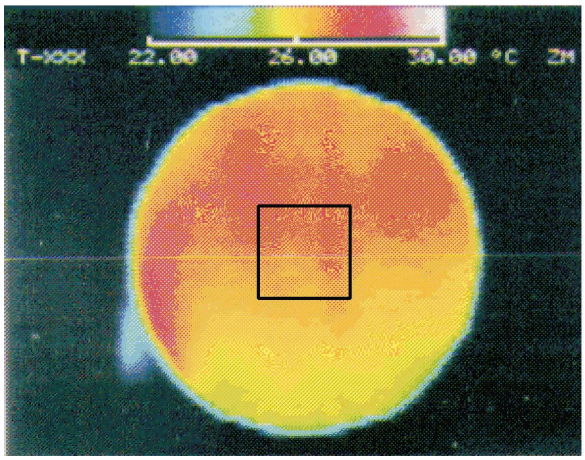

Figure 5. Thermal image of time-averaged radiation energy emitted from the heated fluidizing particles (glass particles, $d = 200$ μm, $U = 1.5U_{\mathrm{mf}}$).

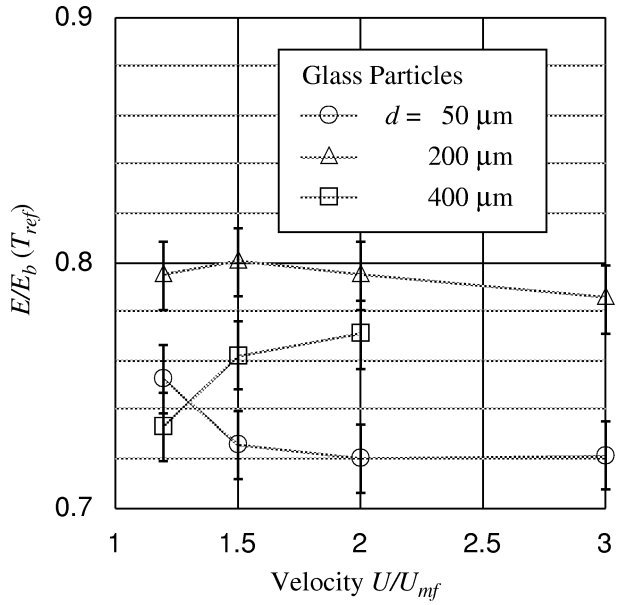

Figure 6. Effect of fluidizing velocity on the dimensionless radiation energy.

part. This is because the generating frequency of bubbles is higher in the lower part than that in the upper part. Also, the bed temperature near the lower part is less. Since the bed temperatureat bottom of the bed is close to the inlet gas temperature T_{in} ($< 25\,^{\circ}\mathrm{C}$; the desired experimental condition), the bed temperature near the lower part does not increase up to 25 °C due to the low inlet gas temperature when the fluidizing particles are not well mixed. Although the bed temperature causes some spatial non-uniformity in the radiation energy, we spatially averaged the radiation energy within the indicated rectangular region to minimize the effect of the temperature non-uniformity on the radiation energy.

Figure 6 shows the dimensionless radiative energy flux versus the fluidizing velocity of glass particles with diameters of 50, 200, and 400 μm. We accounted for the reflected background radiation using the following equation:

$$\frac{E}{E_{\mathrm{b}}(T_{\mathrm{ref}})} = \frac{D}{D_{\mathrm{b}}(T_{\mathrm{ref}})} - (1-\varepsilon_{\mathrm{bed}})\frac{E_{\mathrm{b}}(T_{\mathrm{sur}} = 20\,^{\circ}\mathrm{C})}{E_{\mathrm{b}}(T_{\mathrm{ref}} = 30\,^{\circ}\mathrm{C})} \quad (5)$$

where D and $D_{\mathrm{b}}(T_{\mathrm{ref}})$ are respectively the system output for the radiation energy emitted from the bed and blackbody.

The error bars in *figure 6* represent the whole uncertainties which contain the bias error caused by the uncertainty of $\varepsilon_{\mathrm{bed}}$, and random errors. The magnitude of only the random error is about the size of the symbols. Therefore, it is considered that the decreasing or increasing tendencies of $E/E_{\mathrm{b}}(T_{\mathrm{ref}})$ against fluidizing velocity are reliable, although the whole uncertainties look large.

For the 50 μm particles, the emitted radiation energy $E/E_{\mathrm{b}}(T_{\mathrm{ref}})$ decreases with increasing fluidizing velocity. This is because the residence time of particles on the heat transfer surface correspondingly decreases. Obviously then, as the residence time decreases, the amount of heat received from the surface decreases, and so the emitted radiation energy also decreases.

At a fluidizing velocity greater than $2.0U_{\mathrm{mf}}$, $E/E_{\mathrm{b}}(T_{\mathrm{ref}})$ is almost constant. The reason is considered that the residence time of particles on the heat transfer surface is negligibly small at such large fluidizing velocities, and that the fluidizing particles are heated only by flowing gas in the thermal boundary layer. Since there is no particle that is intensively heated by the direct contact with the surface, this behavior occurs at large fluidizing velocities.

The 400 μm particles showed contrasting results in that $E/E_{\mathrm{b}}(T_{\mathrm{ref}})$ increases as the fluidizing velocity increases, which is due to the non-uniformity of the bed temperature near the bed bottom. When the particle diameter is large at a low fluidizing velocity, the heat diffusion in the bed is considered to be weak. Therefore, the low-temperature region near the bed bottom approaches the lower part of the heat transfer surface (*figure 7*), which decreases $E/E_{\mathrm{b}}(T_{\mathrm{ref}})$. As the fluidizing velocity increases, however, the heat diffusion also increases and

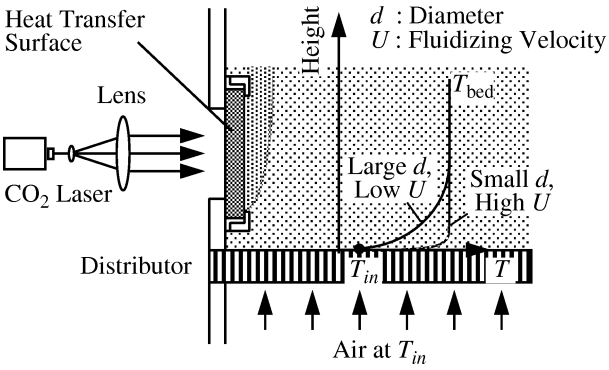

Figure 7. Diagram showing the temperature distribution outside the thermal boundary layer on the heat transfer surface.

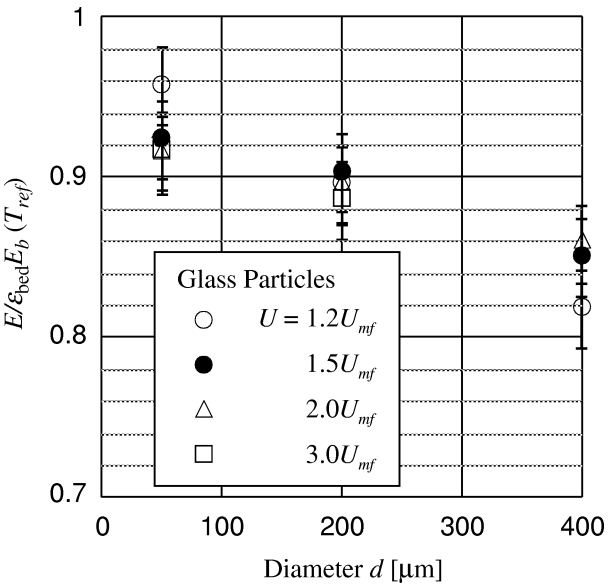

Figure 8. Effect of particle diameter on the dimensionless radiation energy normalized by that emitted from the isothermal bed at the same temperature as the reference blackbody ($T_{ref} = 30\,°C$).

a uniform bed temperature occurs at $T_{bed} = 25\,°C$. Consequently, emitted radiation energy increases as the fluidizing velocity increases. The 200 μm particles showed intermediate behavior between the 50 μm particles and the 400 μm ones.

The results for the 400 μm particles are considered to be peculiar to the present experimental bed, which has the heat transfer surface near the bed bottom. If the particles near the heat transfer surface were not cooled by the inlet gas, the radiation energy emitted by the fluidizing particles would decrease with increasing fluidizing velocity.

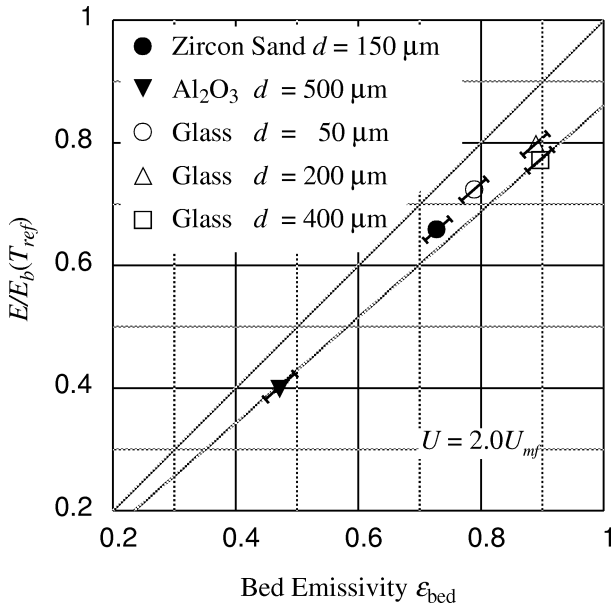

Figure 9. Effect of bed emissivity on the dimensionless radiation energy.

Figure 8 shows the effect of particle diameter on the dimensionless radiation energy emitted from the fluidizing particles. Here the radiation energy is normalized by that emitted from an isothermal fluidized bed at the same temperature as the reference blackbody ($T_{ref} = 30\,°C$). By doing this, we cancel out the amount of emitted radiation energy due to the differences in bed emissivity.

Notice that the normalized radiation energy decreases with increasing particle diameter. That is, as the particle diameter increases, the particle's heat capacity also increases, and therefore, more energy is required to increase its temperature. Moreover, the extinction coefficient of the fluidized bed correspondingly decreases [8]. The optical thickness of the layer where the heated particles exist also decreases, thereby reducing the amount of radiation energy emitted by the heated particles near the heat transfer surface.

Figure 9 shows the effect of bed emissivity on the radiation energy emitted from fluidizing particles at $U = 2.0U_{mf}$, where the radiation energy decreases with decreasing bed emissivity. Here, the magnitude of uncertainty in $E/E_b(T_{ref})$ caused by random errors is about a half size of the symbols. The error bars show the bias error caused by the uncertainty of ε_{bed}. Therefore, the error bars are inclined.

The two lines indicate the limits of the emitted radiation energy from the bed, with the upper and lower line corresponding to the radiation energy emitted from

an isothermal bed at 30 and 25 °C, respectively. Since these temperatures respectively correspond to T_w and T_{bed}, the amount of radiation energy emitted from the fluidizing particles must fall between these lines.

It should be noted that the radiation energy emitted from large particles, such as Al_2O_3 with $d = 500$ μm and glass with $d = 400$ μm, is close to the lower limit, although their bed emissivities are very different. This result suggests that, although there are a few heated particles adjacent to the surface, these particles do not provide a significant amount of additional radiation. In contrast to this, for the beds with small particles, since there are many heated particles near the surface which emit a large amount of additional radiation, the radiation energies are larger than the lower limit. *Figure 9* shows that, although the amount of radiation energy emitted from the fluidizing particles depends on ε_{bed}, the additional radiation emitted from the heated particles depends on the particle diameter.

To clarify the effect of particle diameter on the amount of additional radiation, we consider the additional ratio of the radiation energy, R, given by the following equation:

$$R = \frac{E - \varepsilon_{bed} E_b(T_{bed} = 25\,^\circ\mathrm{C})}{\varepsilon_{bed} E_b(T_w = 30\,^\circ\mathrm{C}) - \varepsilon_{bed} E_b(T_{bed} = 25\,^\circ\mathrm{C})} \quad (6)$$

Figure 10 shows the additional ratio versus the diameter of fluidizing particles. $R = 0$ represents that all the particles are not heated and are in T_{bed} (the lower limit in *figure 9*), and at $R = 1$ they are heated perfectly by the heat transfer surface and are in T_w (the upper limit in *figure 9*). It is found that even though the bed emissivities are different, R decreases monotonically as the particle diameter increases and it is almost independent of ε_{bed}.

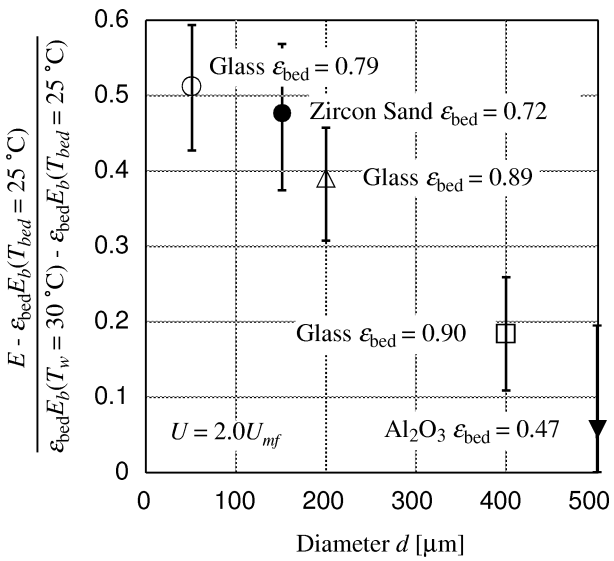

Figure 10. Additional radiation energy produced by the heated particles.

3.3. Applicability to a high-temperature fluidized bed

All experiments were performed at comparatively low temperature where the radiative heat transfer may not be significant. However, we think the present results can be applicable to a fluidized bed operating at a high temperature. In order to demonstrate the applicability of the present results to a high-temperature fluidized bed, we now define the efficiency of the radiation heat transfer, Ψ, as

$$\Psi = 1 - R \quad (7)$$

Using Ψ, for example, as the heat transfer surface is a blackbody and the system is assumed to be one-dimensional, the radiation flux exchanged between the surface and the bed can be predicted by the following equation:

$$E_{net} = \Psi \varepsilon_{bed}\left[E_b(T_w) - E_b(T_{bed})\right] \quad (8)$$

Since Ψ is given by *figure 10*, we can predict the radiation heat transfer for any particle diameters.

Strictly speaking, predicting the radiation heat transfer using equation (8) is limited to a few cases at present, since Ψ also depends on the fluidizing velocities and the thermophysical properties of particles, such as thermal diffusivity. For practical use, we need to determine Ψ for several cases.

However, *figure 10* and equation (8) show that particle diameter is one of the most significant parameters in radiation heat exchange between the fluidizing particles and the heat transfer surface, and that the radiation heat exchange increases with increasing particle diameter. These results would be applicable to any practical fluidized bed with dense phase of particles, and they would be helpful for constructing a model of the radiative heat exchange. A total heat transfer model in fluidized beds including the radiation heat exchange may be constructed in combination with the earlier reported (for example, paper by Molerus [11]) which dealt with other heat transfer modes.

4. CONCLUSION

In order to evaluate the radiation heat exchange occurring in a gas–solid fluidized bed between the fluidizing particles and a heated heat transfer surface, we used an infrared imager to visualize the temperature of fluidizing particles located adjacent to the heated heat transfer surface, as well as to determine the radiation energies emitted from the particles toward the heat transfer surface.

We observed that fluidizing particles are indeed transiently heated by the heat transfer surface, and frequently emit a significant amount of radiation toward the surface. Since the net radiative heat exchange is caused by the difference between the radiation energy emitted from the surface and that emitted from the particles, it is considered that strong radiation toward the surface suppresses the net radiation heat exchange. Therefore, reducing the radiation energy emitted from the fluidizing particles toward the surface is a way to enhance the net radiation heat exchange. This study shows that

(1) using fluidizing particles with a large diameter, and/or

(2) operating the fluidizing bed under high fluidizing velocities

can reduce the radiation energy toward the heat transfer surface. These are effective ways to enhance the net radiative heat exchange for a fluidized bed.

Based on these experimental results, this study has introduced the efficiency of the radiation heat exchange, Ψ, and has demonstrated that the radiation heat exchange between the heat transfer surface and the fluidizing particles can be quantitatively predicted by equation (8) with Ψ. This equation for estimating the net radiation heat exchange shows that using a fluidized bed with high emissivity enhances the net radiation heat exchange.

Acknowledgement

This work was supported in part by the Ministry of Education, Science and Culture of Japan under grant No. 03402030.

REFERENCES

[1] Alavizadeh N., Adams R.L., Welty J.R., Goshayeshi A., An instrument for local radiative heat transfer measurement in a gas-fluidized bed at elevated temperatures, in: The 22nd ASME/AIChE Nat. Heat Transfer Conference, Niagara Falls, 1984.

[2] Basu P., Bed-to-wall heat transfer in a fluidized bed coal combustor, in: Wen C.Y. (Ed.), Fluidization: Application to Coal Conversion Processes, AIChE Symp. Ser. 74 (176) (1978) 187–193.

[3] Il'chenko A.I., Pikashov V.S., Makhorin K.E., Study of radiative heat transfer in a fluidized bed, J. Engrg. Phys. 14 (1968) 32l–324.

[4] Ozkaynak T.F., Chen J.C., Frankenfield T.R., An experimental investigation of radiation heat transfer in a high temperature fluidized bed, in: Kunii D., Toei R., (Eds.), Proc. 4th Int. Conf. Fluidization, Engineering Foundation, New York, 1984, pp. 371–378.

[5] Vadivel R., Vedamurthy V.N., An investigation of the influence of bed parameters on the variation of the local radiative and total heat transfer coefficient around an embedded horizontal tube in a fluidized bed combustor, in: Proc. 6th Int. Conf. Fluidized Bed Combustion, Vol. 3, 1980, pp. 1159–1172.

[6] Zhang H., Xie C., The radiative heat transfer of the immersed tube in a fluidized-bed combustion boiler, in: Proc. 8th Int. Conf. Fluidized Bed Combustion, Vol. 1, 1985, pp. 142–148.

[7] Saxena S.C., Srivastava K.K., Vadivel R., Experimental techniques for the measurement of radiative and total heat transfer in gas fluidized beds: A review, Experimental Thermal and Fluid Science 2 (1989) 350–364.

[8] Yamada J., Kurosaki Y., Satoh I., Shimada K., Radiation heat exchange between a fluidized bed and heated surface, Experimental Thermal and Fluid Science 11 (2) (1995) 135–142.

[9] Tien C.L., Thermal radiation in packed and fluidized beds, Trans. ASME, J. Heat Tran. 110 (4) (1988) 1230–1242.

[10] Yamada J., Kurosaki Y., Estimation for radiative properties of scattering and absorbing media, International Journal of Thermophysics 18 (2) (1997) 547–556.

[11] Molerus O., Mattmann W., Heat transfer mechanisms in gas fluidized beds, Part 1: Maximum heat transfer coefficients, Chemical Engineering Technology 15 (1992) 139–150.

APPENDIX

Uncertainty analysis

The experimental uncertainty indicated in *table I* and the figures are numerically evaluated by the following uncertainty analysis. We will first show the derivation of the uncertainty of the bed emissivity, σ_ε.

In the measurement of the bed emissivity, the temperature of the bed and the heat transfer surface were maintained at 30 °C and the surroundings temperature was controlled at 20 °C. These temperatures fluctuate during the measurements and cause σ_ε. In addition to this, the uncertainty is also caused by the temperature of reference blackbody and the radiation measurements, because the radiation energies emitted from the bed and

the reference blackbody are measured and used for evaluation of σ_ε. Taking account of these elemental error sources, we evaluate σ_ε by using the following equation:

$$\sigma_\varepsilon^2 = \left(\frac{\partial \varepsilon_{\text{bed}}}{\partial D_{\text{iso-bed}}}\right)^2 \sigma_D^2 + \left(\frac{\partial \varepsilon_{\text{bed}}}{\partial D_{\text{b}}(T_{\text{ref}})}\right)^2 \sigma_{D_{\text{ref}}}^2 + \left(\frac{\partial \varepsilon_{\text{bed}}}{\partial T_{\text{bed}}}\right)^2 \sigma_{T_{\text{bed}}}^2 + \left(\frac{\partial \varepsilon_{\text{bed}}}{\partial T_{\text{sur}}}\right)^2 \sigma_{T_{\text{sur}}}^2 + \left(\frac{\partial \varepsilon_{\text{bed}}}{\partial T_{\text{ref}}}\right)^2 \sigma_{T_{\text{ref}}}^2 \quad \text{(A.1)}$$

where σ_D and $\sigma_{D_{\text{ref}}}$ are the uncertainty of radiation measurements for the bed and the reference blackbody, respectively. $\sigma_{T_{\text{bed}}}$, $\sigma_{T_{\text{sur}}}$ and $\sigma_{T_{\text{ref}}}$ are the uncertainty of the temperature of the bed, the surroundings and the reference blackbody, respectively.

The radiation measurements were carried out using the IR imager. Since these measurements are repeated 40 times, and the averaged values of $D_{\text{iso-bed}}$ and $D_{\text{b}}(T_{\text{ref}})$ are adopted to estimate the bed emissivity, it is considered σ_D and $\sigma_{D_{\text{ref}}}$ in equation (A.1) are small and the first and second terms on the right-hand side are negligible.

Using equations (1)–(3), the derivative in the third term of equation (A.1) can be rewritten as

$$\left|\frac{\partial \varepsilon_{\text{bed}}}{\partial T_{\text{bed}}}\right| = \left|\frac{\partial \varepsilon_{\text{bed}}}{\partial E_{\text{b}}(T_{\text{bed}})}\right| \cdot \left|\frac{\partial E_{\text{b}}(T_{\text{bed}})}{\partial T_{\text{bed}}}\right| = \left|\frac{C\varepsilon_{\text{bed}}/D_{\text{b}}(T_{\text{ref}})}{1 - E_{\text{b}}(T_{\text{sur}} = 20\,^\circ\text{C})/E_{\text{b}}(T_{\text{ref}} = 30\,^\circ\text{C})}\right| \cdot \left|\frac{\partial E_{\text{b}}(T_{\text{bed}})}{\partial T_{\text{bed}}}\right| = \left|\frac{\varepsilon_{\text{bed}}/E_{\text{b}}(T_{\text{ref}})}{1 - E_{\text{b}}(T_{\text{sur}} = 20\,^\circ\text{C})/E_{\text{b}}(T_{\text{ref}} = 30\,^\circ\text{C})}\right| \cdot \left|\frac{\partial E_{\text{b}}(T_{\text{bed}})}{\partial T_{\text{bed}}}\right| \quad \text{(A.2)}$$

Using the calibration table of the IR imager, the magnitude of the derivative can be calculated as

$$\left|\frac{\partial \varepsilon_{\text{bed}}}{\partial T_{\text{bed}}}\right|_{T_{\text{bed}}=30\,^\circ\text{C},\ T_{\text{sur}}=20\,^\circ\text{C},\ T_{\text{ref}}=30\,^\circ\text{C}} = 0.115\varepsilon_{\text{bed}}\ [\text{K}^{-1}] \quad \text{(A.3)}$$

In the same manner as above, the derivatives of the forth and fifth terms in equation (A.1) are given as, respectively,

$$\left|\frac{\partial \varepsilon_{\text{bed}}}{\partial T_{\text{sur}}}\right| = \left|\frac{\partial \varepsilon_{\text{bed}}}{\partial E_{\text{b}}(T_{\text{sur}})}\right| \cdot \left|\frac{\partial E_{\text{b}}(T_{\text{sur}})}{\partial T_{\text{sur}}}\right| = \left|\frac{(1 - \varepsilon_{\text{bed}})/E_{\text{b}}(T_{\text{ref}})}{1 - E_{\text{b}}(T_{\text{sur}} = 20\,^\circ\text{C})/E_{\text{b}}(T_{\text{ref}} = 30\,^\circ\text{C})}\right| \cdot \left|\frac{\partial E_{\text{b}}(T_{\text{sur}})}{\partial T_{\text{sur}}}\right| \quad \text{(A.4)}$$

$$\left|\frac{\partial \varepsilon_{\text{bed}}}{\partial T_{\text{sur}}}\right|_{T_{\text{bed}}=30\,^\circ\text{C},\ T_{\text{sur}}=20\,^\circ\text{C},\ T_{\text{ref}}=30\,^\circ\text{C}} = 0.085(1 - \varepsilon_{\text{bed}})\ [\text{K}^{-1}] \quad \text{(A.5)}$$

and

$$\left|\frac{\partial \varepsilon_{\text{bed}}}{\partial T_{\text{ref}}}\right| = \left|\frac{\partial \varepsilon_{\text{bed}}}{\partial E_{\text{b}}(T_{\text{ref}})}\right| \cdot \left|\frac{\partial E_{\text{b}}(T_{\text{ref}})}{\partial T_{\text{ref}}}\right| = \left|\frac{-(\varepsilon_{\text{bed}}E_{\text{b}}(T_{\text{bed}}) + (1 - \varepsilon_{\text{bed}})E_{\text{b}}(T_{\text{sur}}))/E_{\text{b}}(T_{\text{ref}})^2}{1 - E_{\text{b}}(T_{\text{sur}} = 20\,^\circ\text{C})/E_{\text{b}}(T_{\text{ref}} = 30\,^\circ\text{C})}\right| \cdot \left|\frac{\partial E_{\text{b}}(T_{\text{ref}})}{\partial T_{\text{ref}}}\right| \quad \text{(A.6)}$$

$$\left|\frac{\partial \varepsilon_{\text{bed}}}{\partial T_{\text{ref}}}\right|_{T_{\text{bed}}=30\,^\circ\text{C},\ T_{\text{sur}}=20\,^\circ\text{C},\ T_{\text{ref}}=30\,^\circ\text{C}} = 0.115(0.7 - 0.3\varepsilon_{\text{bed}})\ [\text{K}^{-1}] \quad \text{(A.7)}$$

Substituting equations (A.3), (A.5) and (A.7) into equation (A.1) and giving $\sigma_{T_{\text{bed}}}$, $\sigma_{T_{\text{sur}}}$ and $\sigma_{T_{\text{ref}}}$, the whole uncertainty of the bed emissivity σ_ε can be calculated. The elemental errors observed through the entire experiments are $\sigma_{T_{\text{bed}}} = \pm 0.2$ K, $\sigma_{T_{\text{sur}}} = \pm 0.5$ K and $\sigma_{T_{\text{ref}}} = \pm 0.1$ K. The resultant uncertainties for ε_{bed}, which are calculated by using these values, are shown in *table I*.

The error bars (the whole uncertainty) in *figures 6, 8–10* are evaluated by the same manner as described above. In the evaluations, the uncertainty for the temperature of the heat transfer surface, which is necessary to evaluate the whole uncertainty, was given by $\sigma_{T_{\text{w}}} = \pm 0.1$ K.